Up-wave surface elevation for smooth hydrodynamic control of wave energy conversion in irregular waves

Umesh A. Korde
Department of Mechanical Engineering
South Dakota School of Mines and Technology
Rapid City, SD 57701, USA.
Email: Umesh.Korde@sdsmt.edu

***Abstract*—Real-time smooth reactive control and optimal damping of wave energy converters in irregular waves is difficult in part because the radiation impulse response function is real and causal, which constrains the frequency-dependent added mass and radiation damping according to the Kramers–Kronig relations. Optimal control for maximum energy conversion requires independent synthesis of the impulse response functions corresponding to these two quantities. Since both are non-causal, full cancellation of reactive forces and matching of radiation damping requires knowledge or estimation of device velocity into the future. To address this non-causality and the non-causality of the exciting force impulse response function, the use of up-wave surface elevation has been suggested in the literature for synthesis of the necessary control forces. The overall formulation here draws on draws on this approach and leads to smooth control that is near-optimal given the approximations involved in the time-shifting of the non-causal impulse response functions and the consequent up-wave distances at which wave surface elevation is required. A predominantly heaving submerged device comprised of three vertically stacked discs driving a hydraulic cylinder is studied. Absorbed power performance with the present near-optimal approach is compared with two other cases, (i) when single-frequency tuning is used based on non-real time adjustment of the reactive and resistive loads to maximize conversion at the spectral peak frequency, and (ii) when no control is applied with damping set to a constant value. Simulation results are obtained for wave spectra at different significant wave heights and energy periods representing three locations along the U.S. coastline.**

***Index Terms*—wave energy, irregular waves, wave-by-wave control, up-wave surface elevation**

NOMENCLATURE

$\delta(t)$	Dirac delta function located at $t = 0$
$\eta(\cdot;t)$	Wave surface elevation at point $\cdot$ and time t
$\mu(\infty)$	Infinite-frequency added mass of the three disc body in heave
c_d	Constant damping in the system
D	Power take-off damping in constant damping case
$F_f(t)$	Exciting force in heave on the 3-disc body
$F_r(t)$	Actuator applied force on the 3-disc body
$h_f(t)$	Impulse response kernel for exciting force
$h_r(t)$	Radiation impulse response kernel
H_s	Significant wave height
$h_\lambda(t)$	Inverse Fourier transform of radiation damping $\lambda(\omega)$
$h_\mu(t)$	Inverse Fourier transform of frequency-dependent added mass $\mu(\omega)$
k_h	Steady stiffness in the hydraulic power take-off
m	In-air mass of the 3-disc body
R	Device radius
t_c	Time duration beyond which $h_r(t)$ is truncated to zero
T_e	Energy period
t_f	Time duration beyond which $h_f(t)$ is truncated to zero
v	Heave velocity of the 3-disc body
v_m	Heave velocity under single-frequency tuning control
v_o	Device heave velocity under near-optimal control
$v_{opt}(t)$	Optimal device velocity in heave leading to maximum power absorption
x_A	Distance d up-wave of device
x_B	Device location relative to origin
x_R	Distance d_R up-wave of device

I. INTRODUCTION

Wave energy conversion technology has developed rapidly in recent years, and many devices have matured to the point of full-scale ocean operation [1]. Despite the inherent advantages of greater energy density and less variability, wave energy often proves less cost effective than wind and solar power. Active control of the hydrodynamic response of wave energy devices can potentially enable over 3-5 fold increase in overall efficiency, allowing fewer, structurally efficient, smaller devices to meet the required energy generation targets. This could make wave energy cost competitive in many locations and justify the added expense of providing large reactive forces and short term on-board energy storage.

As pointed out in the literature [2], hydrodynamic control for optimal energy conversion in irregular waves presents fundamental physical difficulties. These arise in part from the fact that a body oscillating in waves also forces the free surface to make its own waves. The radiation impulse response function is causal, which implies that the frequency-dependent added mass and radiation damping satisfy the Kramers–Kronig relations. Optimal control for maximum energy conversion

978-0-933957-40-4 ©2013 MTS

requires independent synthesis of the time-domain impulse response kernels for these two quantities. Both are non-causal, since the 'impedance kernel' corresponding to added mass must be an odd function, and that corresponding to radiation damping an even function. Therefore, real-time generation of the control force requires knowledge or estimation of device velocity into the future. Compromise solutions using velocity estimation based on time-series analysis of past velocities were reported several years ago [3], [4].

An alternative time-domain latching type control approach using real-time application of clutching and declutching forces has been investigated since the mid-seventies by many authors [5], [6], [7], [8], [9], [10], etc. Recently, the use of a high-pressure hydraulic power take-off was studied for a heaving buoy type device to optimize the converted hydraulic power in the time domain [11]. For a small, tubular oscillating water column device, a 'non-predictive' phase control strategy was considered more recently [12], with the understanding that the radiation impedance was small. Frequency domain 'complex-conjugate control' approaches comprising adjustable reactive loading for selective tuning to changing wave spectra have been studied since the mid-seventies [13], [14], [15], etc. Such an approach was tested recently on the Wavestar device in Denmark [16].

A method based on a coupled fuzzy logic–robust controller was used for short term tuning with incoming-wave prediction [17]. Some recently proposed time-domain control approaches were evaluated in [18]. A stochastic control approach based on past information only was recently investigated and found to produce good performance relative to optimal time-domain control [19]. 'Hard' displacement and force constraints on the primary converter make it necessary but challenging to find a practical optimal control strategy in the time domain, and a Kalman-filter based predictor was used to derive a time-domain constrained optimal controller for a heaving buoy device [20]. The effect of device geometry on the 'prediction horizon' for real-time control was studied with a view to velocity/exciting force prediction [21].

This paper adopts the approach first discussed in [2] and later outlined in [22] to infer the necessary velocity values from free surface elevation information 'up-wave' of the device (i.e. to the left of the device for waves propagating from left to right). For up-wave distances on the order of 1000 m, a deterministic understanding of wave propagation may be valid (especially where a predominant wave direction is present) [22], [23], [24], etc. Thus, X-band radar technology has been applied in recent years for real-time wave profile measurements at a distance of 500–1500 m for use in ship motion predictions (ahead of offshore operations such as helicopter landing) [24]. LIDAR technology has also been considered for such measurements [25].

A single-mode device with unconstrained oscillations is used here so as to enable greater insight into potential difficulties with such control. The primary energy converter is a submerged body comprised of three vertically stacked discs. Power absorption and control are by means of a double-acting hydraulic cylinder which uses a deeply submerged mass as a reference.

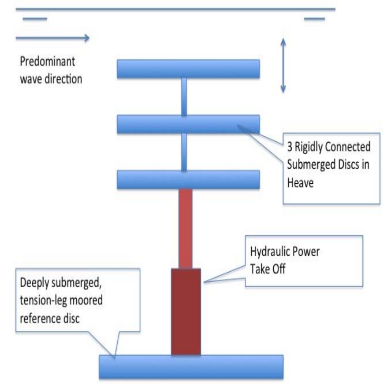

Fig. 1. Schematic view of the device being investigated here.

It was found in an earlier work [26] that the exciting force and hydrodynamic coefficient variations became flatter and more 'broad band' with increasing depth, leading to narrower inverse Fourier transforms in the time domain. As discussed later, this is advantageous because the nature of these functions determines the up-wave distance at which the wave surface elevation is needed, and shorter distances imply greater validity of the present approach and more economical remote sensing measurement hardware (e.g. a lower-power X-band radar) in a practical implementation. Performance of the control based on up-wave surface elevation is compared with single-frequency tuning, where a reactive load component cancelling the inherent + frequency-dependent reactance and a resistive component matching the radiation damping at the peak frequency is used. The performance is also compared with a case where no control is used and constant damping is applied.

Section II following this introduction discusses the overall formulation and the rationale behind the method. Section III describes the purpose of the up-wave surface elevation measurements and the corresponding distances. Section IV derives the impulse response functions leading to device response under control. Simulation procedure for a number of 2-parameter spectra is described in section VI. Results for the three cases are discussed in section VII, and the main findings are summarized in section VIII.

II. Overview of Method

The device used in this work consists of three submerged discs of radius 1 m and stacked at a spacing of 1 m on a single central axis (Figure 1). With this stack configuration heave motion is expected to predominate. A double-acting hydraulic cylinder reacting against an approximately stationary deeply submerged mass utilizes the disc heave for energy generation. This submerged device is used here because results for exciting force and hydrodynamic coefficients are readily available using the method of [27], and because it was found that deeper submergence allowed shorter lengths of time beyond which the radiation and exciting force kernels tended to zero [26]. The equation of motion for heave velocity in an irregular wave train is,

$$\begin{aligned}[m+\mu(\infty)]\,\dot{v}+c_d v+\int_0^{\infty} h_r(\tau)v(t-\tau)d\tau \\ +\,k_h\int_{-\infty}^{t} v(\tau)d\tau=F_f+F_r\end{aligned} \tag{1}$$

where the convolution integral on the left represents the radiation force in heave, due to the waves created by device oscillation near the free surface. The radiation impulse response function/kernel $h_r(t)$ is causal in that only the past and present velocity affects the radiation force. In other words, $h_r(t)=0, t<0$. This implies that its Fourier transform $H(i\omega)$ is analytic in the upper half of the complex-frequency plane [28]. Further, since $h_r(t)$ is real-valued (velocity and radiation force being real-valued), $H_r(-i\omega)=H_r^*(i\omega)$. With

$$\int_{-\infty}^{\infty} h_r(t)\mathrm{e}^{-i\omega t}dt=H_r(i\omega)=\lambda(\omega)+i\omega(\mu(\omega) \tag{2}$$

where $\lambda(\omega)$ and $\mu(\omega)$ are the frequency-dependent radiation damping and added mass respectively. Since $H_r(-i\omega)=H_r^*(i\omega)$, $\lambda(\omega)$ is an even function and $\omega\mu(\omega)$ is an odd function. Further, since both $\lambda(\omega)$ and $\mu(\omega)\to 0$ as $\omega\to\infty$, it can be shown that, for a real-valued ω,

$$PV\int_{-\infty}^{\infty}\frac{H_r(i\varpi)}{\varpi-\omega}d\varpi=\pi i H_r(i\omega) \tag{3}$$

which implies that

$$\begin{aligned}\lambda(\omega)&=\frac{1}{\pi}PV\int_{-\infty}^{\infty}\frac{\varpi\mu(\varpi)}{\varpi-\omega}d\varpi\\ \omega\mu(\omega)&=-\frac{1}{\pi}PV\int_{-\infty}^{\infty}\frac{\lambda(\varpi)}{\varpi-\omega}d\varpi\end{aligned} \tag{4}$$

where PV denotes principal value. Equation (4) shows the Kramers–Kronig relations [29]. $\lambda(\omega)$ and $\mu(\omega)$ are thus related to each other and

$$h_r(t)=\frac{2}{\pi}\int_0^{\infty}\lambda(\omega)\cos\omega t d\omega=-\frac{2}{\pi}\int_0^{\infty}\omega\mu(\omega)\sin\omega t d\omega \tag{5}$$

and it follows that

$$\begin{aligned}\lambda(\omega)&=\int_0^{\infty}h_r(t)\cos\omega t dt\\ \mu(\omega)&=-\frac{1}{\omega}\int_0^{\infty}h_r(t)\sin\omega t dt\end{aligned} \tag{6}$$

Note that the full Fourier transforms of $\lambda(\omega)$ and $\omega\mu(\omega)$ must be even and odd functions of time and equal in magnitude ($=h_r(t)/2$). Thus,

$$\begin{aligned}h_\lambda(t)&=\frac{1}{2\pi}\int_{-\infty}^{\infty}\lambda(\omega)\mathrm{e}^{i\omega t}d\omega\\ h_\mu(t)&=\frac{1}{2\pi}\int_{-\infty}^{\infty}i\omega\mu(\omega)\mathrm{e}^{i\omega t}d\omega\end{aligned} \tag{7}$$

are both *non-causal*. The exciting force $F_f(t)$ may be written in terms of the wave surface elevation η at the device centroid x_B as

$$F_f(t)=\int_{-\infty}^{\infty}h_f(\tau)\eta(x_B;t-\tau)d\tau \tag{8}$$

With respect to $\eta(x_B;t)$, h_f is not causal, and $h_f(t)\neq 0, t<0$. For maximum energy absorption, the reactive terms in equation (1) need to be externally forced out, and the rate of energy radiation from the device needs to be equaled by the rate of energy absorption by the power take-off. In some cases, such as with the present hydraulic power take-off, the same mechanism may be used for reactive force cancellation and energy absorption. Thus, for maximum power absorption, the force $F_r(t)$ needs to be

$$F_r(t)=[m+\mu(\infty)]\dot{v}+k_h\int_{-\infty}^{t}v(\tau)d\tau+F_c(t) \tag{9}$$

where the first two terms contain the frequency-independent inertia and stiffness effects only, and can be derived in real time using velocity and acceleration measurements at the current instant and no prediction is required. $F_c(t)$ is the part that needs to provide the correct power absorption rate and cancel the remaining reactive effects. $F_c(t)$ is the inverse Fourier transform of $F_c(i\omega)$ where

$$F_c(i\omega)=-[\lambda(\omega)+c_d]v(i\omega)+i\omega\mu(\omega)v(i\omega) \tag{10}$$

Thus,

$$F_c(t)=-c_d v(t)-\int_{-\infty}^{\infty}h_\lambda(\tau)v(t-\tau)d\tau+\int_{-\infty}^{\infty}h_\mu(\tau)v(t-\tau)d\tau \tag{11}$$

Substitution of equations (9) and (11) into equation (1) results in $v(t)\equiv v_{opt}(t)$ with

$$2\left(c_d+\int_{-\infty}^{\infty}h_\lambda(\tau)v_{opt}(t-\tau)d\tau\right)=F_f(t) \tag{12}$$

Equivalently,

$$2\int_{-\infty}^{\infty}[c_d\delta(\tau)+h_\lambda(\tau)]v_{opt}(t-\tau)d\tau=F_f(t) \tag{13}$$

In practice $h_r(t)$ [and therefore $h_\lambda(t)$ and $h_\mu(t)$] $\to 0$ beyond $t\to t_c$, where t_c may be several seconds. Similarly, $h_f(t)\to 0$, $t<-t_{f1}$ and $h_f(t)\to 0$, $t>t_{f2}$, where t_{f1} and t_{f2} may be equal and set to t_f (alternatively, $t_f=\max[t_{f1},t_{f2}]$ may be used). Thus, in practice, the following approximations may be used.

$$F_c(t)\approx -c_d v(t)-\int_{-t_c}^{t_c}h_\lambda(\tau)v(t-\tau)d\tau+\int_{-t_c}^{t_c}h_\mu(\tau)v(t-\tau)d\tau \tag{14}$$

and,

$$F_f(t)=\int_{-t_f}^{t_f}h_f(\tau)\eta(x_B;t-\tau)d\tau \tag{15}$$

To synthesize $F_c(t)$ therefore, estimates of velocity up to $t=t_c$ into the future are required. If the force F_f is used in this estimation, then F_f estimates are required up to $t=t_f$

further into the future (i.e. up to $t = t_c + t_f$). Finally, with $F_c(t)$ approximated as in equation (14), the device dynamics under near-optimal control will reduce to,

$$2\left(c_d + \int_{-t_c}^{t_c} h_\lambda(\tau) v_o(t-\tau) d\tau\right) = F_f(t) \tag{16}$$

where now $v(t)$ is replaced by $v_o(t)$, which is the device velocity under near-optimal control as enabled by $F_r(t)$ based on the approximate $F_c(t)$.

III. Use of Up Wave Surface Elevation

As mentioned previously, a deterministic analysis of propagation in the predominant wave direction may be valid over distances on the order of 1000 m. The surface elevation for a uni-directional wave propagating from left to right over $x > 0$ is described as

$$\eta(x_B; i\omega) = A(i\omega)\mathrm{e}^{-ik(\omega)x_B} \tag{17}$$

where

$$\eta(x_B; t) = \frac{1}{2\pi}\int_{-\infty}^{\infty} \eta(x_B; i\omega)\mathrm{e}^{i\omega t} d\omega \tag{18}$$

The complex amplitude $A(i\omega)$ contains both amplitude and phase information [22]. Ignoring any viscous attenuation effects, if x_A is a point to the left of, i.e. up-wave of x_B, so that $x_B - x_A = d$, then for the frequency ω and wave number $k(\omega)$,

$$\eta(x_B; i\omega) = \mathrm{e}^{-ik(\omega)d}\eta(x_A; i\omega) \tag{19}$$

The time-domain relation between the surface elevations η at $x = x_A$ and $x = x_B$ is generally not causal [2], [22], given the theoretical presence of zero-frequency or infinite-period waves. However, only a range of frequencies is relevant in practical wave spectra, and though longer water waves travel faster, a maximum velocity limit is reached in finite water depth h. Past this limit $(= \sqrt{gh})$, group velocity equals phase velocity and propagation becomes nondispersive and causal[1]. This observation is used to define the time-shifted impulse response functions below and to determine the location of the surface elevation used in control. The exciting force $F_f(i\omega)$ in the frequency domain can be written as

$$F_f(i\omega) = \int_{-\infty}^{\infty} F_f(t)\mathrm{e}^{-i\omega t} dt \tag{20}$$

and equation (8) transforms to,

$$F_f(i\omega) = H_f(i\omega)\eta(x_B; i\omega) \tag{21}$$

where

$$H_f(i\omega) = \int_{-\infty}^{\infty} h_f(t)\mathrm{e}^{-i\omega t} dt \tag{22}$$

is the complex frequency response function for the exciting force. Following arguments similar to [22], one can construct a version $h_{fd}(t)$ of $h_f(t)$ that is right-shifted on the time axis by t_f seconds so that,

$$h_{fd}(t) = h_f(t - t_f) \tag{23}$$

Since h_f is truncated to zero for $t < -t_f$, h_{fd} is approximately causal, or $h_{fd}(t) \approx 0,\ t < 0$. In the frequency domain,

$$H_{fd}(i\omega) = H_f(i\omega)\mathrm{e}^{-ik(\omega)d} \tag{24}$$

where

$$d = v_{max}t_f, \quad \text{where} \quad v_{max} = \sqrt{gh} \tag{25}$$

v_{max} is the fastest wave speed (for the longest wave) in the spectrum at a roughly constant water depth h [22]. From equation (19),

$$\eta(x_A; i\omega) = \mathrm{e}^{ik(\omega)d}\eta(x_B; i\omega) \tag{26}$$

where d is as determined in equation (25). Therefore,

$$F_f(i\omega) = H_f(i\omega)\eta(x_B; i\omega) \approx H_{fd}(i\omega)\eta(x_A; i\omega) \tag{27}$$

Taking the inverse Fourier transform of equation (27),

$$\begin{aligned} F_f(t) &\approx \int_{-t_f}^{t_f} h_f(\tau)\eta(x_B; t-\tau) d\tau \\ &= \int_{0}^{2t_f} h_{fd}(\tau)\eta(x_A; t-\tau) d\tau \end{aligned} \tag{28}$$

$\eta(x_A; t)$ is the surface elevation at a station x_A up-wave of the device. The present and past values of $\eta(x_A; t)$ from 0 to $2t_f$ are required for a good approximation of $F_f(t)$ at the present instant.

The near-optimal control force to be synthesized according to equation (14) has two integrals with non-causal impulse response kernels h_λ and h_μ. Analogously to h_{fd}, the time-shifted versions of h_λ and h_μ can be found as

$$\begin{aligned} h_{\lambda c}(t) &= h_\lambda(t - t_c) \\ h_{\mu c}(t) &= h_\mu(t - t_c) \end{aligned} \tag{29}$$

Since h_λ and h_μ are approximately zero for $|t| > t_c$, $h_{\lambda c}$ and $h_{\mu c}$ are approximately causal, i.e. $\approx 0,\ t < 0$. In light of the above discussion, a distance d_c can be defined in the up-wave direction such that

$$d_c = v_{max}t_c, \quad \text{with} \quad v_{max} = \sqrt{gh} \tag{30}$$

In the frequency domain, this defines two functions,

$$\begin{aligned} \lambda_c(i\omega) &= \lambda(\omega)\mathrm{e}^{-ik(\omega)d_c} \\ \mu_c(i\omega) &= \mu(\omega)\mathrm{e}^{-ik(\omega)d_c} \end{aligned} \tag{31}$$

With the waves propagating from left to right, were the device placed a distance d_c up-wave of its current location x_B at a distance x_C, where $x_C = x_B - d_c$, then, within linearity, its velocity in the frequency domain would be related to the current device velocity according to,

$$v_c(i\omega) = \mathrm{e}^{ik(\omega)d_c}v(i\omega) \tag{32}$$

[1] In case $h \to \infty$, a finite depth h_s may be used for which the exciting and radiation force impulse response functions very closely approach those for infinite depth [22].

In light of equations (31) and (32), the control force $F_c(i\omega)$ in the frequency domain can be expressed as,

$$\begin{aligned} F_c(i\omega) &= -\lambda_c(i\omega)\mathrm{e}^{ik(\omega)d_c}v(i\omega) - c_d v(i\omega) \\ &\quad + i\omega\mu_c(i\omega)\mathrm{e}^{ik(\omega)d_c}v(i\omega) \\ &= -\lambda_c(i\omega)v_c(i\omega) - c_d v(i\omega) + i\omega\mu_c(i\omega)v_c(i\omega) \end{aligned} \quad (33)$$

which in the time domain takes the form,

$$\begin{aligned} F_c(t) = &- \left(c_d v_c(t) + \int_0^{2t_c} h_{\lambda c}(\tau)v_c(t-\tau)d\tau \right) \\ &+ \int_0^{2t_c} h_{\mu c}(\tau)v_c(t-\tau)d\tau \end{aligned} \quad (34)$$

where the two impulse response kernels $h_{\lambda c}$ and $h_{\mu c}$ are causal to the degree of approximation implied in equation (14). The velocity under near-optimal control in the frequency domain can be expressed as,

$$v_o(i\omega) = \frac{H_{fd}(i\omega)\eta(x_A;i\omega)}{2[c_d + \lambda(\omega)]} \quad (35)$$

If the device were a distance d_c up-wave of the location x_B,

$$v_{oC}(i\omega) = v_o(i\omega)\mathrm{e}^{ik(\omega)d_c} \quad (36)$$

Defining x_R as a station d_c up-wave of $x_A(= x_B - d)$, such that $x_R = x_A - d_c$,

$$\eta(x_A;i\omega) = \mathrm{e}^{-k(\omega)d_c}\eta(x_R;i\omega) \quad (37)$$

implying that,

$$v_{oC}(i\omega) = \frac{H_{fd}(i\omega)\eta(x_R;i\omega)}{2[c_d + \lambda(\omega)]} \quad (38)$$

In the time domain, this can be expressed as

$$v_{oC}(t) = \int_0^{2t_R} h_{oC}(\tau)\eta(x_R;t-\tau)d\tau \quad (39)$$

where

$$h_{oC}(t) = \frac{1}{2\pi}\int_{-\infty}^{\infty} \frac{H_{fd}(i\omega)}{2[c_d + \lambda(\omega)]}\mathrm{e}^{i\omega t}d\omega \quad (40)$$

is causal to the approximation implicit here, and $t_R = t_f + t_c$. Further, $x_R = x_B - d - d_c = x_B - d_R$,

$$d_R = v_{max}(t_f + t_c) = v_{max}t_R, \quad \text{with} \quad v_{max} = \sqrt{gh} \quad (41)$$

Generation of the near-optimal $F_c(t)$ therefore requires use of the surface elevation information a distance d_R up-wave of the device.

IV. Forces Synthesized

In a response simulation in the time domain according to equation (1) or in experimental testing, it is straightforward, knowing the physical parameters of the device and its infinite-frequency added mass in heave to construct the causal part of the control force as,

$$F_s(t) = [m + \mu(\infty)]\dot{v}(t) + k_h\int_{-\infty}^{t} v(\tau)d\tau \quad (42)$$

Application of this force requires real time measurement of the device velocity (at least). With F_s applied, the device velocity in the frequency domain is,

$$[i\omega\mu(\omega) + \lambda(\omega) + c_d]v(i\omega) = F_f(i\omega) + F_c(i\omega) \quad (43)$$

$F_c(i\omega)$ may be constructed based on the second of equations (33). Using the 'desired' $v_o(i\omega)$ and $v_{oC}(i\omega)$ to generate $F_c(i\omega)$,

$$\begin{aligned} F_c(i\omega) = &\frac{[i\omega\mu_c(i\omega) - \lambda_c(i\omega)]H_{fd}(i\omega)}{2[c_d + \mu(\omega)]}\eta(x_R;i\omega) \\ &- \frac{c_d H_{fd}(i\omega)}{2[c_d + \lambda(\omega)]}\eta(x_A;i\omega) \end{aligned} \quad (44)$$

Substituting (44) into equation (43), and solving for $v(i\omega) \equiv v_{act}(i\omega)$,

$$\begin{aligned} v_{act}(i\omega) = &\frac{[c_d + 2\lambda(\omega)]H_{fd}(i\omega)}{2[c_d + \lambda(\omega)][i\omega\mu(\omega) + \lambda(\omega) + c_d]}\eta(x_A;i\omega) \\ &+ \frac{[i\omega\mu_c(i\omega) - \lambda_c(i\omega)]H_{fd}(i\omega)}{2[c_d + \lambda(\omega)][i\omega\mu(\omega) + \lambda(\omega) + c_d]}\eta(x_R;i\omega) \end{aligned} \quad (45)$$

Introducing the impulse response functions $h_A(t)$ and $h_R(t)$

$$\begin{aligned} h_A(t) &= \frac{1}{2\pi}\int_{-\infty}^{\infty} \frac{[c_d + 2\lambda(\omega)]H_{fd}(i\omega)}{2[c_d + \lambda(\omega)][i\omega\mu(\omega) + \lambda(\omega) + c_d]}\mathrm{e}^{i\omega t}d\omega \\ h_R(t) &= \frac{1}{2\pi}\int_{-\infty}^{\infty} \frac{[i\omega\mu(\omega) - \lambda(\omega)]H_{fd}(i\omega)}{2[\lambda(\omega) + c_d][i\omega\mu(\omega) + \lambda(\omega) + c_d]}\mathrm{e}^{i\omega t}d\omega \end{aligned} \quad (46)$$

$v_{act}(t)$ in the time domain can be evaluated as

$$\begin{aligned} v_{act}(t) = &\int_0^{2t_f} h_A(\tau)\eta(x_A;t-\tau)d\tau \\ &+ \int_0^{2t_f} h_R(\tau)\eta(x_R;t-\tau)d\tau \end{aligned} \quad (47)$$

If the present simulations work correctly, $v_{act}(t)$ must be nearly identical to $v_o(t)$. In a practical implementation any difference between v_{act} and v_o arising from disturbances could be corrected using negative feedback based on the difference (and its derivative and integral if needed). However, a controller leading to maximum power absorption will still need v_{oC} up-wave (or future-velocity estimates such as based on time-series models) as, in a sense, a 'feedforward' input.

The part of the control force F_c responsible for power absorption can be expressed in the frequency domain as,

$$F_l(i\omega) = -\frac{\lambda_c(i\omega)H_{fd}(i\omega)}{2[c_d + \lambda(\omega)]}\eta(x_R;i\omega) - \frac{c_d H_{fd}(i\omega)}{2[c_d + \lambda(\omega)]}\eta(x_A;i\omega) \quad (48)$$

so that, in the time domain,

$$\begin{aligned} F_l(t) = &-\int_0^{2t_R} h_{l1}(\tau)\eta(x_R;t-\tau)d\tau \\ &- \int_0^{2t_f} h_{l2}(\tau)\eta(x_A;t-\tau)d\tau \end{aligned} \quad (49)$$

The impulse response functions h_{l1} and h_{l2} can be found as follows.

$$h_{l1}(t) = \frac{1}{2\pi}\int_{-\infty}^{\infty}\frac{\lambda_c(\omega)H_{fd}(i\omega)}{2[c_d+\lambda(\omega)]}\mathrm{e}^{i\omega t}d\omega$$
$$h_{l2}(t) = \frac{1}{2\pi}\int_{-\infty}^{\infty}\frac{c_d H_{fd}(i\omega)}{2[c_d+\lambda(\omega)]}\mathrm{e}^{i\omega t}d\omega \tag{50}$$

The reactive part of $F_c(t)$ can be written in the frequency domain as,

$$F_a(i\omega) = \frac{i\omega\mu_c(i\omega)H_{fd}(i\omega)}{2[c_d+\lambda(\omega)]}\eta(x_R;i\omega) \tag{51}$$

and in the time domain as,

$$F_a(t) = \int_0^{2t_R} h_a(\tau)\eta(x_R;t-\tau)d\tau \tag{52}$$

where

$$h_a(t) = \frac{1}{2\pi}\int_{-\infty}^{\infty}\frac{i\omega\mu_c(i\omega)H_{fd}(i\omega)}{2[c_d+\lambda(\omega)]}\mathrm{e}^{i\omega t}d\omega \tag{53}$$

V. Wave Surface Elevation at x_R and x_A

As mentioned earlier, radar-based non-contact measurement techniques may be used to obtain the real-time surface elevation at x_R and x_A [23], [24], etc. In case significant reflections from the device or shore exist, measurements at at least two additional points in the predominant propagation direction would be needed for separation of the incident and reflected wave components at x_A and x_R. In the present simulations, the surface elevations at x_R and x_A are generated numerically. Phase angle is generated at $x = x_R$ using a random number generator over $[0, 2\pi]$. Two-parameter Pierson–Moskowitz type spectra are fitted to observed wave parameters at 3 U.S. coastal locations: (i) National Data Buoy Center (NDBC) station 51207 in Kaneohe Bay (water depth 100 m), Hawaii: $H_s = 2.4$ m, $T_e = 9.0$ s; (ii) NDBC station 44017 at Montauk Point off New York (water depth, 52 m): $H_s = 2.6$ m, $T_e = 10.8$ s; and (iii) NDBC station 46239 at Point Sur off California (water depth 366 m): $H_s = 1.4$ m, $T_e = 14.0$ s. Note that these conditions are not annual averages but rather conditions observed at the time of the calculation. Further, even though a Pierson–Moskowitz type spectrum appears to fit the Kaneohe Bay and Montauk point data, it does not fully capture the somewhat bimodal spectrum at Point Sur at the time of observation. For the spectral density $S(\omega)$ inferred from the above H_s and T_e, the wave amplitude $A(\omega)$ is,

$$A(\omega) = \sqrt{\frac{S(\omega)}{2}} \tag{54}$$

which is consistent with the inverse Fourier transformation procedure used here for computing $\eta(x;t)$. Thus, the surface elevation at x_R is generated using

$$\eta(x_R;t) = \frac{1}{2\pi}\int_{-\infty}^{\infty}A(\omega)\mathrm{e}^{-i[k(\omega)x_R-\omega t+\theta(\omega)]}d\omega \tag{55}$$

where $\theta(\omega)$ is the random phase angle mentioned above. The surface elevation at x_A is computed as

$$\eta(x_A;t) = \frac{1}{2\pi}\int_{-\infty}^{\infty}A(\omega)\mathrm{e}^{-i[k(\omega)x_A-\omega t+\theta(\omega)]}d\omega \tag{56}$$

VI. Simulations

Time domain calculations were performed for the present submerged 3-disc device with disc radius R of 1 m and disc vertical spacing of 1 m. Submergence depth of the topmost disc was 2 m, to prevent loss of static submergence up to wave amplitudes approaching 2 m. The hydraulic power take-off was assumed to be capable of generating the large control forces required in swell-dominated irregular waves. Energy storage was also assumed to be available near the device, so that the required reactive power could be supplied. For small devices such as the present device, the need for large control forces and energy storage represents a design challenge.

The exciting force and hydrodynamic coefficients in heave were computed as discussed in [30]. A disc thickness of 0.2 m was used for each disc, and a steady stiffness k_h =10 kN/m was used for the hydraulic power take-off. The depth h was as specified above for the three locations, except that where it exceeded 225 m, a value $h = 225$ m was used.

A program developed within Matlab was used to simulate the velocity response in the present wave conditions. The standard Discrete Fourier transformation routine in Matlab was used here for the various inverse Fourier transform calculations. For each spectrum, the response was computed over 10 minutes. $v_{act}(t)$ and $v_o(t)$ were compared over this duration. For the control forces applied, $v_{act}(t)$ was plotted alongside $F_f(t)$ to test whether velocity was synchronous with exciting force. Also computed was the average power absorbed over the 10-minute interval, and this was compared with the incident power at the given H_s and T_e. The device response and absorbed power were also found when (i) single-frequency tuning control was used, where the forces were tuned to cancel the reactive terms and match the radiation damping at the spectral peak frequency; and when (ii) just constant linear damping was applied with no active control. In the case with single-frequency tuning, the device velocity in heave could be expressed in frequency domain as,

$$v_m(i\omega) = \frac{H_{fd}(i\omega)\eta(x_A;i\omega)}{i\omega[\mu(\omega)-\mu_o]+[\lambda(\omega)+\lambda_o+2c_d]} \tag{57}$$

where μ_o is the frequency-dependent added mass at the peak frequency in the spectrum, and λ_o is the frequency-dependent radiation damping for the device at the peak frequency. No measurement of $\eta(x_A;t)$ is required for this case in practice, and only periodic updating of the incoming-wave spectrum is needed (as implemented in [16]). The simulation here uses it simply as a means to evaluate the time domain velocity $v_m(t)$ within the existing formulation. Thus, in the time domain,

$$v_m(t) = \int_0^{2t_f} h_{fc}(\tau)\eta(x_A;t-\tau)d\tau \tag{58}$$

where

$$h_{fc}(t) = \frac{1}{2\pi}\int_{-\infty}^{\infty} \frac{H_{fd}(i\omega)}{i\omega[\mu(\omega)-\mu_o]+[\lambda(\omega)+\lambda_o+2c_d]}\mathrm{e}^{i\omega t}d\omega \tag{59}$$

For the case with constant damping D and no active control, the velocity in the time domain is,

$$v_{nc}(t) = \int_0^{2t_f} h_{nc}(\tau)\eta(x_A; t-\tau)d\tau \tag{60}$$

where

$$h_{nc}(t) = \frac{1}{2\pi}\int_{-\infty}^{\infty} H_{nc}(i\omega)\mathrm{e}^{i\omega t}d\omega \tag{61}$$

where

$$H_{nc}(i\omega) = \frac{H_{fd}(i\omega)}{i\omega[m+\mu(\infty)+\mu(\omega)]-i(1/\omega)k+[\lambda(\omega)+c_d+D]} \tag{62}$$

The incident power in kW incident over the device diameter $2R$ for a given H_s and T_e combination was found using

$$P_{inc} = 0.49H_s^2T_e(2R) \tag{63}$$

The average power absorbed in the three cases could be found over a simulation duration of $[0, T]$ seconds as follows.

$$P_w = \frac{1}{T}\int_0^T [F_l(t)+c_d v_{act}(t)]v_{act}(t)dt \tag{64}$$

for near optimal control. For single-frequency tuning,

$$P_f = \frac{1}{T}\int_0^T [\mu_o + c_d]v_m^2(t)dt \tag{65}$$

With no control and constant damping,

$$P_{nc} = \frac{1}{T}\int_0^T Dv_{nc}^2(t)dt \tag{66}$$

The simulation used discrete-time approximations for the various continuous-time expressions in this treatment. The sampling period was linked to the calculation time window (and frequency range).

VII. Discussion

It is seen that h_r (and consequently h_λ and h_μ) $\to 0$ beyond $t \to 5.5$ s, and $h_f \to 0$ beyond $|t| \to 4$ s, and these values are used, respectively, as t_c and t_f here for the determination of distances d_c and d and the synthesis of the near-optimal control forces [30]. The impulse response functions h_{nc}, h_{fc}, and h_o are also discussed in [30]. h_{fc} need not be used in practice for the single-frequency tuning control if the power take-off is simply continually re-tuned to different frequencies based on measurements of the incoming spectra at a point in the vicinity of the device. This process only requires a look-up table with known frequency distributions of the added mass and radiation damping along with the terms comprising the fully-causal $F_s(t)$. Re-tuning may be carried out at 10-15 minute intervals (e.g. as in [16]). Surface elevation from $x = x_A$ is used for finding the $v_o(t)$ at the current instant. h_o is used in these simulations simply to obtain v_o for comparison with the v_{act} resulting from the applied control forces.

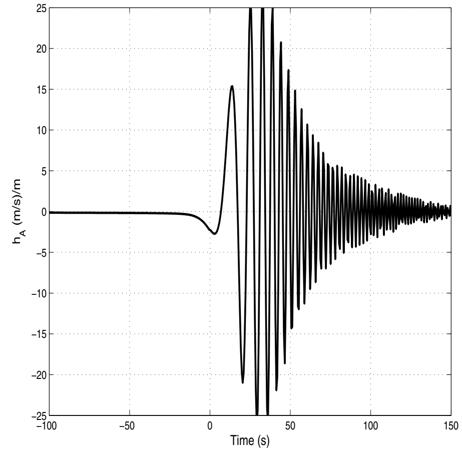

Fig. 2. Impulse response function h_A used in evaluating device velocity.

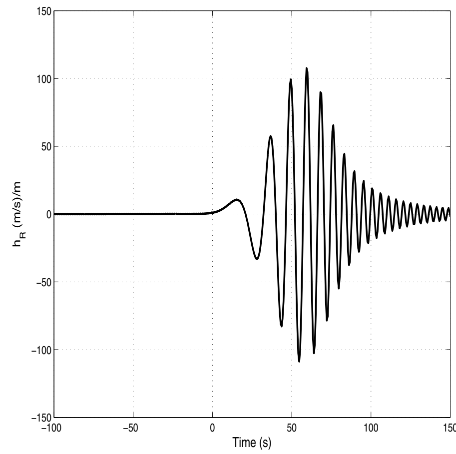

Fig. 3. Impulse response function h_R used in evaluating device velocity.

Figures 2 and 3 show the impulse response kernels h_A and h_R [equations (46)]. Both are seen to be nearly causal with respect to the surface elevation information they each receive [$\eta(x_A; t)$ for h_A and $\eta(x_R; t)$ for h_R]. The impulse response functions h_{l1} and h_{l2} are shown in Figures 4 and 5 and are also seen to be almost causal. These kernels have a long memory, however, which is likely due to the highly oscillatory phase variation introduced by the $\mathrm{e}^{-k(\omega)d}$ (and like) operators. It is recalled that for the left $\to$ right propagating waves here this substitutes for the Fourier transform of the time-shift operator subject to the arguments in section III, [2] and [22]. The greater the up-wave distance, the more sensitive the phase angle becomes to k. As mentioned, this work uses the standard Discrete Fourier transformation in Matlab, but alternative approaches including a purely time-domain implementation with nested convolutions need to be considered. The wave profiles at x_R and x_A are generated using equations (55) and (56) respectively. Figure 7 shows the velocity v_{act} resulting from the force applied based on h_A and h_R. This matches the desired v_o very closely once the control

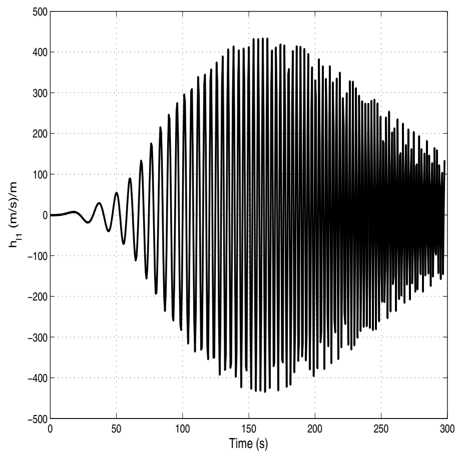

Fig. 4. Impulse response function h_{l1} used in evaluating control force.

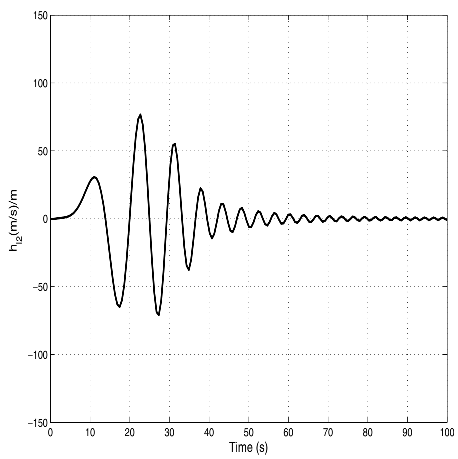

Fig. 5. Impulse response function h_{l2} used in evaluating control force.

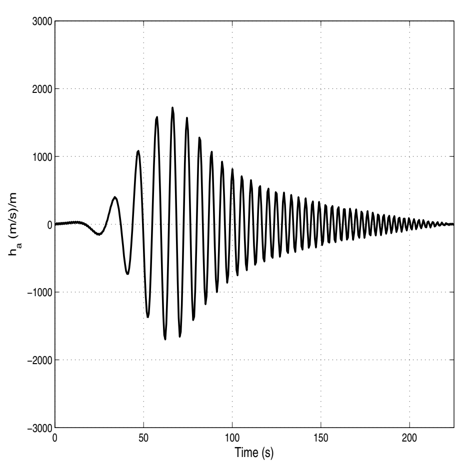

Fig. 6. Impulse response function h_a used in evaluating control force.

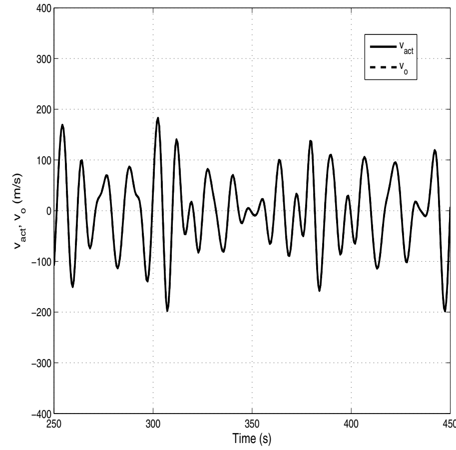

Fig. 7. Velocity resulting from forces and desired velocity under near-optimal control.

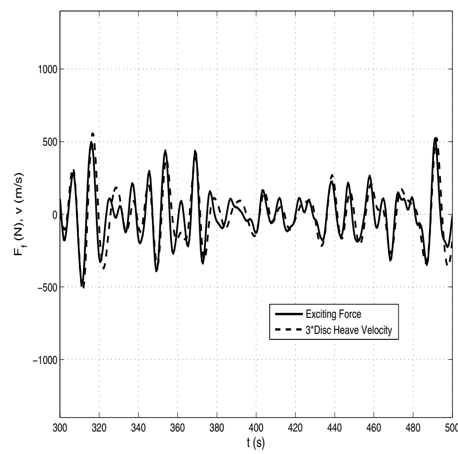

Fig. 8. Exciting force and velocity v_{act} under near-optimal control.

force is fully synthesized. The heave exciting force and device heave velocity are shown in Figure 8. The velocity seems to be synchronous with the force for the most part, although small differences exist, which may have resulted from an incomplete synthesis of the terms used to compute v_{act} and F_f and errors in the inverse Fourier transformations.

Figures 9–11 plot the absorbed power over 10 minutes at the three locations. Note that the vertical-axis units are different for the top two figures than for the bottom figure. Near-optimal control provides the best power absorption of the three cases. Some negative values are observed, as also noted in [2]. These are likely largely due to the inherent approximations in the numerical routines being used in the number of inverse Fourier transformations used in arriving at these results. As seen here, peak-frequency tuning control enables a reasonably good performance. Constant damping without control leads to almost negligible power absorption for this submerged device [31]. The following summarizes the 10-minute mean powers in the three cases at the three locations (recall that the disc is submerged 2 m below the surface, and that the incident-wave effects decrease exponentially with depth).

- $H_s = 1.4$ m; $T_e = 14.0$ s (Point Sur, CA; NDBC 46239;

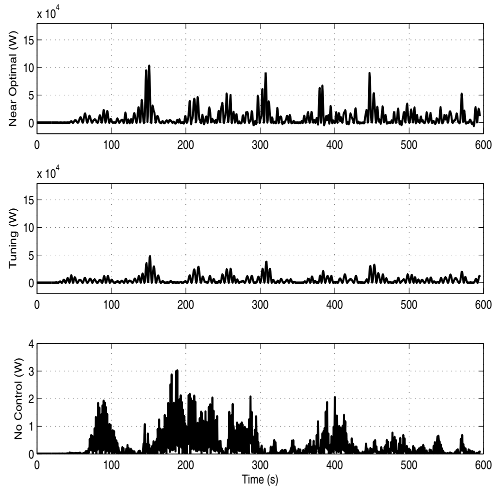

Fig. 9. Instantaneous power absorbed in the three cases studied. (i) Top: near-optimal control; (ii) Middle: peak-frequency tuning; (iii) Bottom: constant damping, no active control. Note that the vertical scale for the bottom plot different from that for the top two.

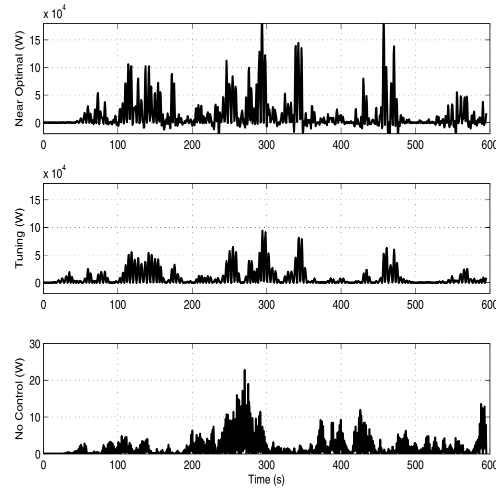

Fig. 10. Instantaneous power absorbed in the three cases studied. (i) Top: near-optimal control; (ii) Middle: peak-frequency tuning; (iii) Bottom: constant damping, no active control. Note that the vertical scale for the bottom plot different from that for the top two.

July 11, 2013 AM): $P_{inc} = 26.9$ kW; P_{wc} (10-minute average)= 8.8 kW (efficiency: 32.5 %); P_{fc} (10-minute average) = 4.8 kW (efficiency: 18%); P_{nc} = 0.3 W.

- $H_s = 2.4$ m; $T_e = 9.0$ s (Kaneohe Bay, HI; NDBC 51207; July 11, 2013 AM): $P_{inc} = 50.8$ kW; P_{wc} (10-minute average)= 14.1 kW (efficiency: 28.0 %); P_{fc} (10-minute average) = 8.7 kW (efficiency: 17%); P_{nc} = 1.8 W.
- $H_s = 2.6$ m; $T_e = 10.8$ s (Montauk Point, NY; NDBC 44017; March 8, 2013 PM): $P_{inc} = 71.5$ kW; P_{wc} (10-minute average)= 24.3 kW (efficiency: 34.0 %); P_{fc} (10-minute average) = 13.7 kW (efficiency: 19%); P_{nc} = 1.8 W.

Greatest 10-minute average conversion efficiency is seen to be dependent on the energy period, but seems greater for longer energy periods in general [30]. This is desirable, as greater energy is available in the swell-dominated spectra. This does imply a need for greater control forces and greater stored energy, however. Simulations such as these should be carried out for wave parameters observed throughout the year for a better assessment of annual productivity. The average reactive power spent in near-optimal control at each location was found to be 1–2 % of the average power absorbed. This should ideally equal actuator power losses which are ignored here. Hence, this non-zero average appears to be due to numerical inaccuracies.

VIII. Conclusion

The main goal of this study has been to investigate a close approximation to real-time optimal control of a wave energy converter. Wave surface elevation up-wave of the device was used as discussed in the formulations of [2] and [22]. Control was applied to cancel out the reactive forces acting on the device and to match the radiation damping in irregular waves.

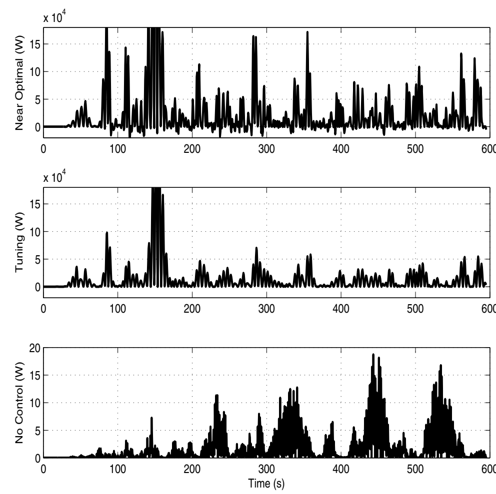

Fig. 11. Instantaneous power absorbed in the three cases studied. (i) Top: near-optimal control; (ii) Middle: peak-frequency tuning; (iii) Bottom: constant damping, no active control. Note that the vertical scale for the bottom plot different from that for the top two.

In the approach followed here, the predominant wave direction is thought to be from left to right over $x > 0$, and wave surface elevation is measured at an up-wave distance determined using (i) the time shift required to make the inverse Fourier transform of the radiation damping approximately causal, (ii) the time shift needed to make the inverse Fourier transform of the exciting force variation approximately causal, and (iii) the maximum wave propagation speed at the water depth of operation at which propagation becomes non-dispersive.

A submerged device comprised of three vertically stacked discs was used, since greater submergence was recently found to require shorter up-wave distances at which wave surface elevation was needed. The problem of evaluating the control force and the resulting device velocity was formulated using a combination of derived impulse response functions operating on the free surface elevation at two up-wave stations. Simulations were carried out in 'fitted' wave spectra at three US coastal locations. Such simulations need to be performed in a large number of wave conditions observed over an entire year for a better assessment of annual productivity increase with control. The velocity under control (termed 'near-optimal' due to the necessary approximations implied in (i), (ii), and (iii) above) and the control force were computed over time values ranging from 0 to 600 s. The wave profile at the two stations was here synthesized numerically. The velocity was plotted alongside exciting force over 600 s, and the two were found to be nearly synchronous. The absorbed power was also computed at each instant and averaged over the simulation duration. Results were compared with two other conditions: (i) when single-frequency tuning was used to set the reactive force and power take-off damping to provide reactive force cancellation and radiation damping match at the peak frequency in a spectrum, and (ii) when no control was used, with damping maintained at a constant value.

Device velocity was unconstrained in this work, but constraints may be applied in practice by introducing deliberate errors in the impulse response functions used in synthesizing the control force. Such errors may be programmed to increase with the approaching significant wave heights once they exceed a known energy capture limit. Given the large forces involved in near-optimal control, energy storage on-board or near the device may be required. Such storage would be particularly important for small devices if they are efficiently to convert large amounts of energy from swell-dominated wave spectra. A convenient way to measure wave surface elevation would be to use a radar type remote sensing technique designed to provide this information in real time.

ACKNOWLEDGMENT

I am grateful to Larry and Linda Pearson for their support through the Pearson endowment.

REFERENCES

[1] A. F. de O Falcão, "Wave energy utilization: a review of the technologies," *Renewable and Sustainable Energy Reviews*, vol. 14, pp. 899–918, 2010.

[2] S. Naito and S. Nakamura, "Wave energy absorption in irregular waves by feedforward control system," in *Proc. IUTAM Symp. Hydrodynamics of Wave Energy Utilization*, D. V. Evans and A. F. de O. Falcão, Eds. Springer Verlag, Berlin, 1985, pp. 269–280.

[3] U. A. Korde, "Efficient primary energy conversion in irregular waves," *Ocean Engineering*, vol. 26, pp. 625–651, 1999.

[4] U. A. Korde, M. P. Schoen, and F. Lin, "Strategies for time-domain control of wave energy devices in irregular waves," in *Proc. 11th Int. Soc. Offshore and Polar Engr. (ISOPE) Conference*, 2002, stavanger, Norway.

[5] K. Budal and J. Falnes, "Interacting point absorbers with controlled motion," in *Power from Sea Waves*, B. Count, Ed. Academic Press, London, 1980, pp. 381–399.

[6] R. E. Hoskin, B. M. Count, N. K. Nichols, and D. A. C. Nicol, "Phase control for the oscillating water column," in *Proc. IUTAM Symp. Hydrodynamics of Wave Energy Utilization*, D. V. Evans and A. F. de O. Falcão, Eds. Springer Verlag, Berlin, 1985, pp. 257–268.

[7] A. F. de O. Falcão and P. A. P. Justino, "Owc wave energy devices with air flow control," *Ocean Engineering*, pp. 1275–1295, 1999.

[8] J. N. B. A. Perdigao and A. J. N. A. Sarmento, "A phase control strategy for owc devices in irregular waves," pp. 205–209, 1989.

[9] A. Babirat and A. H. Clement, "Optimal latching control of a wave energy device in regular and irregular waves," *Applied Ocean Research*, vol. 28, no. 2, pp. 77–91, 2006.

[10] U. A. Korde, "Phase control of floating bodies from an on-board reference," *Applied Ocean Research*, vol. 23, pp. 251–262, 2001.

[11] A. F. de O. Falcão, "Phase control through load control of oscillating body wave energy converters with hydraulic pto system," *Ocean Engineering*, vol. 35, pp. 358–366, 2008.

[12] M. F. P. Lopes, J. Hals, R. P. F. Gomes, T. Moan, L. M. C. Gato, and A. F. de O. Falcão, "Experimental and numerical investigation of non-predictive phase control strategies for a point absorbing wave energy converter," *Ocean Engineering*, vol. 36, pp. 386–402, 2009.

[13] S. H. Salter, "Development of the duck concept," in *Proc. Wave Energy Conference*, 1978, heathrow, U.K.

[14] P. Nebel, "Maximizing the efficiency of wave-energy plants using complex conjugate control," *Proc. IMechE Part I - Journal of Systems and Control Engineering*, vol. 206, no. 4, pp. 225–236, 1992.

[15] U. A. Korde, "A power take-off mechanism for maximizing the performance of an oscillating water column wave energy device," *Applied Ocean Research*, vol. 13, no. 2, pp. 75–81, 1991.

[16] R. H. Hansen and M. M. Kramer, "Modeling and control of the wave star prototype," in *Proc. 9th European Wave and Tidal Energy Conference*, 2011, southampton, UK, paper 163.

[17] M. P. Schoen, J. Hals, and T. Moan, "Wave prediction and robust control of heaving wave energy devices for irregular waves," *IEEE Trans. Energy Conversion*, vol. 26, no. 2, pp. 627–638, 2011.

[18] J. Hals, J. Falnes, and T. Moan, "A comparison of selected strategies for adaptive control of wave energy converters," *J. Offshore Mechanics and Arctic Engineering*, vol. 133, no. 3, pp. 1–12, 2011.

[19] J. T. Scruggs, S. M. Lattanzio, A. A. Taflanidis, and I. I. Cassidy, "Optimal causal control of a wave energy converter in a random sea," *Applied Ocean Research*, vol. 42, pp. 1–15, 2013.

[20] J. Hals, J. Falnes, and T. Moan, "Constrained optimal control of a heaving buoy wave energy converter," *J. Offshore Mechanics and Arctic Engineering*, vol. 133, no. 1, pp. 1–15, 2011.

[21] F. Fusco, J.-C. Gilloteaux, and J. Ringwood, "A study on the prediction requirements in time domain control of wave energy converters," in *Proc. Control Applications in Marine Systems*, Germany, 2010.

[22] J. Falnes, "On non-causal impulse response functions related to propagating water waves," *Applied Ocean Research*, vol. 17, no. 6, pp. 379–389, 1995.

[23] M. R. Belmont, J. M. K. Horwood, R. W. F. Thurley, and J. Baker, "Filters for linear sea-wave prediction," *Ocean Engineering*, vol. 33, no. 17–18, pp. 2332–2351, 2006.

[24] J. Dannenberg, P. Naaijen, K. Hessner, H. den Boom, and K. Reichert, "The on board wave and motion estimator owme," in *Proc. Int. Soc. Offshore and Polar Engr. Conf.*, 2010.

[25] M. R. Belmont, J. M. K. Horwood, R. W. F. Thurley, and J. Baker, "Shallow angle wave profiling lidar," *J. Atmospheric and Oceanic Technology*, vol. 24, no. 6, pp. 1150–1156, 2007.

[26] U. A. Korde and R. C. Ertekin, "An open water submerged device for wave energy focusing and conversion," in *10th European Wave and Tidal Energy Conference*, 2013, aalborg, Denmark; submitted.

[27] P. A. Martin and L. Farina, "Radiation of water waves by a heaving submerged horizontal disc," *J. Fluid Mechanics*, vol. 337, pp. 365–379, 1997.

[28] J. V. Wehausesn, "Causality and the radiation condition," *J. Engineering Mathematics*, vol. 26, pp. 153–158, 1992.

[29] E. R. Jeffreys, "Simulation of wave power devices," *Applied Ocean Research*, vol. 6, no. 1, pp. 31–39, 1984.

[30] U. A. Korde, "On using up-wave surface elvation for efficient wave energy conversion in irregular waves," 2013, preprint.

[31] U. A. Korde and R. C. Ertekin, "On wave energy conversion and focusing in open water," *Renewable Energy*, 2013, in press.